Soft Matter

Cite this: *Soft Matter*, 2011, **7**, 8977

www.rsc.org/softmatter

PAPER

Homo- and hetero-interactions between air bubbles and oil droplets measured by atomic force microscopy†

Rico F. Tabor,[ab] Chu Wu,[bc] Hannah Lockie,[ab] Rogerio Manica,[d] Derek Y. C. Chan,[bce] Franz Grieser[bf] and Raymond R. Dagastine*[ab]

Received 31st May 2011, Accepted 12th July 2011
DOI: 10.1039/c1sm06006f

The atomic force microscope was used to analyse the interactions between bubbles and oil droplets in surfactant-free aqueous solutions. Both homo- (bubble-bubble and drop-drop) and hetero- (bubble-drop) interactions were examined to elucidate the role of colloidal and hydrodynamic forces which, together with interfacial deformations dictate the stability in these systems. It is shown that electrical double-layer forces can be rendered attractive within a small pH range, and that the Van der Waals force can be switched from attractive to repulsive by material choice and ionic strength through salt effects on the so-called 'zero-frequency' term of the Lifshitz theory. By measuring interaction events between bubbles and drops at higher velocities, it is seen that deformation of the bodies and lubrication in the film generated between them can be predicted with a continuum hydrodynamic theory. These results suggest that solution pH and droplet material choice can be used to enhance or inhibit coalescence in such multi-component and multi-phase systems, and this may prove useful in controlling the behaviour of systems in microfluidics, as well as dispersion and formulation science.

Introduction

Interactions between droplets of oil and gas bubbles are central to tuning the desired properties during the manufacture of foodstuffs such as ice cream and mousse,[1] cosmetics and pharmaceuticals, and in mineral flotation and separation.[2] The interactions in such multi-component and multi-phase systems affect static properties such as shelf-life, as well as dynamic properties such as mouthfeel and texture. However, the possibility of homo- and hetero- interactions which can occur means that their analysis and formulation represents a significant theoretical and experimental challenge. Additionally, these systems tend to be decorated with surfactant or polymer stabilisers, which further complicate the interactions. Recently, bubble-drop systems have attracted interest in the field of microfluidics, where their ability to 'pair' or coalesce but remain immiscible is of use.[3,4] In these cases, the droplets and bubbles tend to be 'naked', or free of stabilisers. The forces which control this behaviour are still however incompletely understood.

Owing to their ubiquity in emulsions and foams, analysing the interactions between deformable oil droplets and bubbles in water has attracted considerable attention in recent years.[5–7] Thus far, this research has focused on the homo-case. The homo-interaction between two emulsion droplets or bubbles in aqueous solution can be quantified in terms of the Derjaguin-Landau-Verwey-Overbeek (DLVO) theory, developed originally to understand the stability of dispersions of solid particles. For homo-interactions, the surface forces comprise repulsive electrical double-layer (EDL) and attractive Van der Waals (VdW) forces. It has even been possible to analyze and model dynamic interactions between such deformable objects with quantitative precision, whereby lubrication in the thin aqueous film between the interacting interfaces is a key feature.[5,8,9]

However, for the hetero-system of a droplet and bubble interacting through an intervening aqueous phase, the scenario becomes more complex, as the bodies may deform to different extents,[10] and the DLVO forces can be attractive or repulsive, depending upon the material and charging properties of the liquid phases and interfaces.

In addition to the classical DLVO interaction, there may be a short-range hydrophobic force that acts between hydrophobic entities in aqueous solutions at very small separations.[11] This short-range hydrophobic interaction attraction is significant when surfaces are brought to within separations of a few water molecules diameter or less. It has been suggested to be entropic in origin, relating to the preferred orientation of water molecules at

[a]*Department of Chemical and Biomolecular Engineering, University of Melbourne, Parkville 3010, Australia. E-mail: rrd@unimelb.edu.au*
[b]*Particulate Fluids Processing Centre, University of Melbourne, Parkville 3010, Australia*
[c]*Department of Mathematics and Statistics, University of Melbourne, Parkville 3010, Australia*
[d]*Institute of High Performance Computing, 138632, Singapore*
[e]*Faculty of Life and Social Sciences, Swinburne University of Technology, Hawthorn 3122, Australia*
[f]*School of Chemistry, University of Melbourne, Parkville 3010, Australia*
† Electronic supplementary information (ESI) available. See DOI: 10.1039/c1sm06006f

hydrophobic interfaces.[12] This interaction is often cited as being responsible for folding interactions in proteins, but should also be expected to operate at similar separations between all hydrophobic surfaces. It is important to distinguish this short-range interaction from the apparent long-range hydrophobic force that has been suggested to exist between hydrophobised solid surfaces in water and extends over 100 nm or more.[13,14] In our present experiments, we see no evidence for such a long-range interaction.

When a droplet and bubble interact, they may either remain as discrete bodies during and after the interaction when a repulsive force dominates, or a coalescence event may occur when attraction dominates. In the case of coalescence, because the bodies are immiscible, one can engulf or partially engulf the other, or a lens can form. In each case, an air-oil interface is formed. If one body is immobilised on a solid substrate - which is always the case in the experiments presented here - then the coalescing body will form a floating lens on the immobilised body, and this can be observed using optical microscopy. The geometry of this final state will be controlled by the interfacial and surface energies of the various interfaces within the 3-phase system,[15] and whether or not the contact line of the surface-immobilised body is 'pinned' in place, or able to move.

In this work, we use the atomic force microscope (AFM) to undertake a detailed study of the interactions between an air bubble and droplets of hydrocarbon or fluorocarbon oils. We explore separate regions where hydrodynamic drainage forces and equilibrium surface forces dominate. In order to provide a full 'tool-kit' with which to analyse these systems, homo-measurements were also made between pairs of droplets and bubbles. The results suggest that both material choice and solution conditions can be used to enhance or inhibit coalescence between dissimilar colloids.

Materials and methods

Materials

Tetradecane (TD) and perfluorooctane (PFO) were obtained from Sigma (99%), and purified by column chromatography over Florisil (Sigma). Their purity was determined by drop-shape analysis tensiometry (DataPhysics OCA tensiometer), giving equilibrium interfacial tension values of 54.2 ± 0.5 mN m^{-1} for TD and 50.5 ± 0.5 mN m^{-1} for PFO. Solution pH was adjusted by addition of concentrated nitric acid or sodium hydroxide solution (both from Sigma, used as received). Deionised water was from a Milli-Q system, with minimum resistivity 18.4 MΩ cm. Before use, all glass surfaces were cleaned sequentially in 10% Ajax detergent, then 10% nitric acid, and finally 10% sodium hydroxide, each step being followed by rinsing with copious amounts of deionised water.

Bubbles were generated using an ultrasonic transducer (Undatim Ultrasonics D-reactor), at a frequency of 515 KHz, and power of 25 W. The substrates used for bubble generation were glass Petri dishes that had been cleaned and then partially hydrophobised through an esterification reaction in absolute ethanol for 2 h.[16] This was found to generate a surface of intermediate hydrophobicity that was appropriate for immobilising bubbles, but which allowed them to be readily picked up by the AFM cantilever. The contact angle of bubbles on this substrate was found to be around 60°. For measurements involving PFO, droplets of the oil were generated using a 100 μL syringe to disperse a few μL of the oil under water in a 6 cm Petri dish.[9] For TD experiments, droplets were generated by nebulising the oil with a glass syringe over a surface composed of 100 nm of gold which had been deposited on a glass cover slip (Menzel-Gläser 22 × 22 mm, #1 thickness) using an Emitech K575x sputter coater, with an intermediate layer of 10 nm of chromium as an adhesion promoter. This surface was then modified by immersion in a 1 mM solution of 1-decanethiol in ethanol. The observed macroscopic contact angles of TD and PFO on these substrates in water were 90° and 155° respectively.

AFM measurements

Rectangular silicon AFM cantilevers (450 × 50 × 3 μm) were custom made, with a circular gold region (diameter 45 μm, thickness ≈ 20 nm) added at ≈ 2 μm from the end by focused ion-beam deposition (Fig. 1).[17,18] Cantilever spring constants, K, were determined by the method of Hutter and Bechhoeffer.[19] The AFM measurements were performed on an Asylum MFP-3D AFM, equipped with a linear variable differential transformer (LVDT) sensor in the Z-movement direction, to allow direct detection of cantilever Z-position during force measurements. This has been shown to be vital for accurate dynamic force-displacement measurements, as the instantaneous velocity of the piezo drive is not constant.[17]

Bubbles and droplets used for measurements had diameters in the range 80–150 μm. Interaction events were measured by using the AFM cantilever to pick one bubble or droplet up, and driving this towards a substrate-immobilised bubble or droplet at a nominally constant speed until either coalescence occurred, or until a fixed deflection of the cantilever was reached in the case of stable, repulsive interactions.[7] The effects of surface forces were examined at low speeds (0.2 μm s^{-1}) where hydrodynamic effects are negligible.[8] To measure dynamic interactions where hydrodynamics are important, much higher velocities in the range 10–100 μm s^{-1} were used. Deflection of the cantilever was measured by the optical lever method, and converted to a force using the cantilever spring constant. Experiments were arranged and

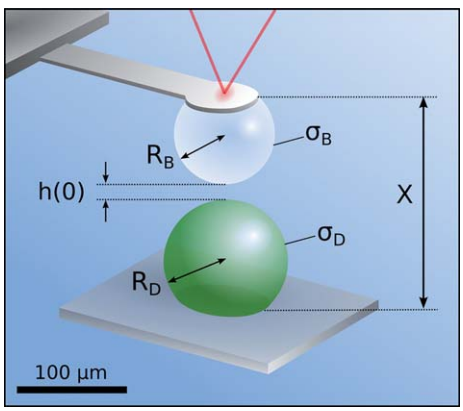

Fig. 1 Schematic of the experimental set-up, showing a bubble on the cantilever positioned above a surface-immobilised drop. Relevant parameters and dimensions are labeled, and defined in the text below.

followed with high-magnification optical microscopy from below (Nikon TE2000, 40x objective). This allowed a precise measurement of bubble radii to be made with a tolerance of ±2 μm. A micro-positioning system was used to align the surface-immobilised bubble or droplet below the cantilever-attached bubble or droplet. This alignment was essential to ensure that the interactions were axisymmetric, which is a requirement in obtaining reproducible data for theoretical analysis.[5,18]

Theoretical modeling

A theoretical model was used to predict both the quasi-static data, where hydrodynamics is negligible and surface forces dominate, and the dynamic data, where high collision velocities were used and hydrodynamics plays an important role in determining the force experienced by the drops and bubbles. This model has been presented in considerable detail in previous work.[7,8,10,20] When dealing with two deformable objects with different interfacial tensions, minor modifications are required. This version of the model has been described by Chan *et al.*,[7,10] but the key changes are also detailed here. The harmonic mean, σ of interfacial tensions of the water-air bubble, σ_b and water-oil droplet, σ_d: $\sigma = (2\sigma_b\sigma_d)/(\sigma_b + \sigma_d)$ is used to define the capillary number, $Ca = \mu V\sigma$, where μ is the dynamic viscosity of water and V is the characteristic drive velocity.

The asymptotic boundary condition was also altered slightly to take into account the two interfacial tensions. The scaled asymptotic boundary condition at radial position $r = r_{max}$ is expressed as:

$$\frac{\partial h}{\partial t} + \frac{\partial F}{\partial t}M = \frac{\partial X}{\partial t} \tag{1}$$

where h is the film thickness, F the force, and X the separation between the cantilever and surface. The function M is expressed as:

$$M = \frac{1}{2\sigma_b}\left[\log\left(\frac{r_{max}}{2R_b}\right) + B_b\right] + \frac{1}{2\sigma_d}\left[\log\left(\frac{r_{max}}{2R_d}\right) + B_d\right] \tag{2}$$

where Rd and Rb are the droplet and bubble radii. B_b and B_d are expressed as:

$$B_i = 1 + \frac{1}{2}\cdot\log\left(\frac{1+\cos\theta_i}{1-\cos\theta_i}\right) \tag{3}$$

where $i = b, d$ and θ_b and θ_d are the contact angle of the bubble on the cantilever, and droplet on the surface (both in water) respectively. These expressions assume that the contact line that the droplet and bubble make on the surfaces on which they are immobilised is pinned (*i.e.*, unable to move during interactions) which is always observed in these experiments.

In order to obtain individual predicted deformations for the droplet and bubble at various time points during dynamic interactions, a slight extension to the model was used. A general equation that describes the bubble/droplet profile, z, is:

$$z_i(r,t) = R_i(1-\cos\theta_i) - \frac{r^2}{2R_i} + \alpha_i(r,t) \tag{4}$$

where $i = b, d$ for bubble or droplet, and $\alpha(r, t)$ is the deformation of the bubble/droplet. For small deformations, that are appropriate to the present experiments, the drop profile given by the linearised Young-Laplace equation is:[10]

$$-\frac{\sigma_i}{r}\frac{\partial}{\partial r}\left(r\frac{\partial z_i}{\partial r}\right) = \frac{2\sigma_i}{R_i} - (\Pi + p) \tag{5}$$

where Π is the disjoining pressure in the film due to surface forces, and p is the hydrodynamic pressure in the film, relative to the bulk pressure. Substituting eqn (4) into the linearised Young-Laplace equation gives:

$$\frac{\partial}{\partial r}\left(r\frac{\partial \alpha_i}{\partial r}\right) = \frac{r}{\sigma_i}(\Pi + p) \tag{6}$$

This equation may be integrated to give:

$$\alpha(r) = \alpha(r_{max}) + r_{max}\left(\frac{\partial \alpha}{\partial r}\right)_{max}\log\left(\frac{r}{r_{max}}\right) - \frac{1}{\sigma_i}\int_r^{r_{max}}(\Pi + p)\log\left(\frac{r}{r'}\right)r'\,dr' \tag{7}$$

$\alpha(r_{max})$ can be found by using the analytical solution for the outer region which is applicable for $r = r_{max}$,[10] and $(\partial\alpha_i/\partial r)_{r_{max}}$ can be found by using the boundary condition $(\partial\alpha_i/\partial r) \to 0$ as $r \to 0$. This gives:

$$\left(\frac{\partial \alpha_i}{\partial r}\right)_{r_{max}} = \frac{1}{\sigma_i r_{max}}\int_0^{r_{max}} r(\Pi + p)\,dr \tag{8}$$

Results and discussion

By utilising results from the homo-bodied drop-drop and bubble-bubble experiments before considering the hetero-bodied case, a complete picture of the surface charging behaviour of all of the components was obtained, in addition to an understanding of the Van der Waals interactions (which dominate when charge interactions are minimal, *e.g.*, close to the isoelectric point) within the system.

Van der Waals interactions

The retarded Hamaker functions for the material combinations encountered in the experiments presented here were calculated using Lifshitz theory,[21] and are shown in Fig. 2. For the calculations, the dielectric function of water was taken from Dagastine *et al.*[22] and for tetradecane from Hough and White.[23] Dielectric data for PFO was estimated by a linear extrapolation of the UV and IR oscillator strengths from the data given for C_5 to C_7 perfluorocarbons in the work of Drummond *et al.*[24] Dielectric data for all of the materials used are given in the ESI.† The two homo-droplet systems (TD and PFO mutually interacting through water) are expected to experience a relatively small, attractive force corresponding to a positive Hamaker function, as the difference between the dielectric functions of the oils and water is low. The air-water-PFO interaction is also attractive, with a Hamaker function that tends to a slightly larger magnitude at all separations.

Interestingly, the Hamaker function for air-water-TD shows unusual behaviour. The first term in the Lifshitz summation (the so-called 'zero-frequency' term) includes Keesom and Debye dipolar contributions,[25] and hence is related to the large value of

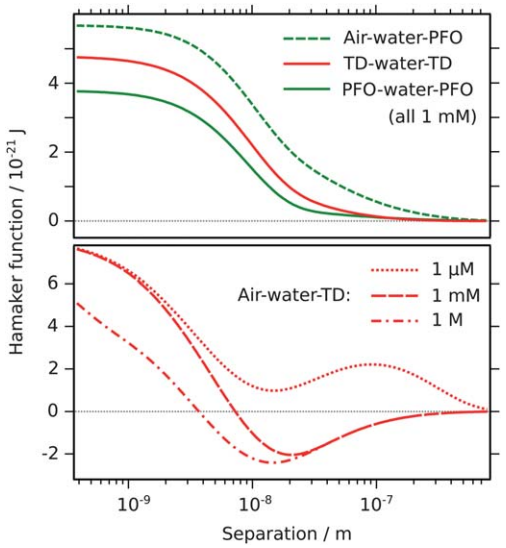

Fig. 2 Top: Hamaker functions for material combinations used in these experiments, calculated using Lifshitz theory, as described in the text. The calculations are for an effective ionic strength of 1 mM, which partially screens the zero-frequency term arising from the dipolar contributions of water. Bottom: the effect of ionic strength on the Hamaker function for air-water-TD.

the static permittivity of water. In the present system, this term makes a large attractive contribution at low ionic strengths, but its magnitude will be screened with the addition of salt.[26] Thus at a separation of ≈ 10 nm, the air-water-TD Hamaker function is positive (corresponding to attraction) at low ionic strength, but becomes negative (corresponding to repulsion) as ionic strength is increased. This change of sign and magnitude suggests another possible method by which interactions between materials can be controlled and manipulated. It is clear that this behaviour is highly dependent on the dielectric data for water. For comparison, Hamaker functions were also calculated for air-water-TD in various salt conditions using the spectral construction for water of Parsegian and Weiss,[27] and the Cauchy form given by Hough and White.[23] The overall form of the Hamaker functions are similar for each water spectrum, and agreement at larger separations is good, although the magnitudes at smaller separations differ somewhat. These results are included in the ESI.† It is worth noting that the predicted Van der Waals forces experienced by these systems are an order of magnitude smaller than, for example, two bubbles interacting in water (where the limiting value of the Hamaker function is 5.2×10^{-20} J at small separations),[7] or many air-water solid interactions.[28]

Electrical double-layer interactions and surface charging

The surface potentials of oil droplets were obtained by using the AFM to measure the force experienced during the approach of two like droplets at low speed, shown for PFO in Fig. 3. By fitting the data to the expected force calculated using the Chan-Dagastine-White model,[7,29,30] which accounts for both surface forces and deformation of the droplets, it was possible to extract the surface potentials. In this fitting procedure, the only 'free' parameter is the surface potential, as droplet radii, contact angles and interfacial tensions were measured experimentally, and a full

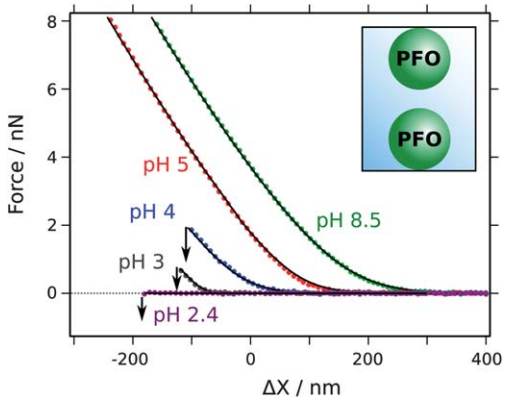

Fig. 3 Effectively equilibrium interactions (at speed = 0.2 μm s^{-1}) between like pairs of PFO droplets in aqueous solutions, measured using AFM. The arrows indicate the point at which coalescence occurred for droplets in solutions at pH 2.4, 3 and 4. Stable interactions were observed for pH 5 and 8.5 up to the maximum applied load of 40 nN; retract branches for these curves are not shown. Symbols are experimental data points, and solid lines are model predictions, calculated using the Chan-Dagastine-White model as described in the text.

retarded Hamaker function was calculated (see above). When the surface potential is low, the film between droplets becomes very thin, and may become thin enough to allow the Van der Waals force to induce coalescence. For such thin films, the force is very sensitive to the surface potential, and hence very accurate values are obtained. Conversely, the force/separation data is relatively insensitive to the thick films preserved by large surface potentials at high pH, and this is reflected in the error bars on the data points in Fig. 4.

The surface potential of air bubbles using this AFM technique has been published previously,[7] and these results were found to be in good agreement with those obtained by electrophoresis.[31] There appears to be very little difference in the charging

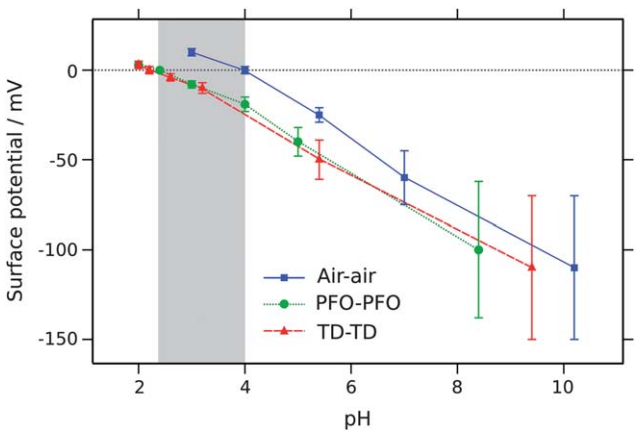

Fig. 4 Surface potentials derived from model fitting the slow approach data for homo-interactions between like pairs of droplets and bubbles. Data for bubbles are taken from previous work.[7] The error bars reflect the sensitivity of the predicted fits to the surface potential. Lines are drawn as a guide to the eye, and the shaded region indicates where the oil droplets and air bubble have different surface charges, and hence would be expected to experience an attraction due to electrical double-layer forces.

behaviour and isoelectric point of hydrocarbon and fluorocarbon droplets. This is consistent with observations by Creux *et al.*,[32] who found the zeta potential of a wide range of different oils to be virtually identical within experimental error. These results may also help to resolve earlier qualitative observations of what were thought to be the anomalous differences in the coalescence behaviours of hydrocarbon and fluorocarbon drops as a function of pH using AFM.[33] Despite apparently similar, low zeta potentials seen for the two drop types in that work (and confirmed in the current study), coalescence behaviour for the two oils differed at low pH. The current work suggests that this may be due to changes in the magnitude of the Hamaker function with electrolyte concentration. Recent improvements in experimental protocol[34] have increased the sensitivity and precision of force measurements with droplets, and hence the current work provides significant quantitative advances.

It is interesting to note that the apparent isoelectric point (IEP) of oil droplets is 1–1.5 pH units lower than that of air bubbles. This could suggest a difference in the affinity of the respective interfaces for the various ionic species in solution. Assuming that the negative charge at the oil-water and air-water interfaces results from strong, specific adsorption of hydroxide ions,[32,35] this may suggest that the oil-water interface has a greater affinity for these ions than does the air-water interface, or that carbon dioxide species are less able to displace hydroxide for oil-water than for air-water interfaces.

Hetero-interactions

From the Hamaker functions presented in Fig. 2, it appears that the sign of the Van der Waals interaction can be modified by material selection and ionic strength. For droplets and bubbles in concentrated salt solutions (where Debye lengths are short and charges are screened), this already suggests a method by which some control over bubble-drop coalescence or pairing could be exerted. Here, 'coalescence' refers to the state in which the bubble and droplet are connected by an air-oil interface (*i.e.*, that no water film remains between them). Additionally, electrical double-layer interactions should also offer some degree of control. Because the isoelectric point of the oil droplets and air bubbles are at different pH values, there is a 'window' of around 1.5 pH units between pH 2.5 and pH 4 (see Fig. 4) in which the sign of the surface potential on the bubbles and drops will be opposite, causing an attraction. Outside of this window, EDL forces will be repulsive. Hence, by small adjustments in solution pH, it should be possible to cause or inhibit coalescence of bubble-drop pairs.

To demonstrate these predicted effects experimentally, interactions between oil droplets and air bubbles were measured in a range of pH and salt conditions. For PFO, these interactions were accurately predicted by inference from the calculated Hamaker functions and measured surface potentials, and are shown in Fig. 5. At pH 3.0, which is within the attractive 'window' where the surface charge of the oil-water and air-water interfaces are of different sign, a pure attraction between the bubble and droplet is seen, resulting in coalescence. Just outside of this region, at pH 4.5, a slight repulsion due to electrical double-layer repulsion is observed. As the droplet and bubble come closer however, the film thins sufficiently such that the Van der Waals attraction causes coalescence. At higher pH values, thick films are maintained by the more highly charged interfaces, resulting in stable interactions.

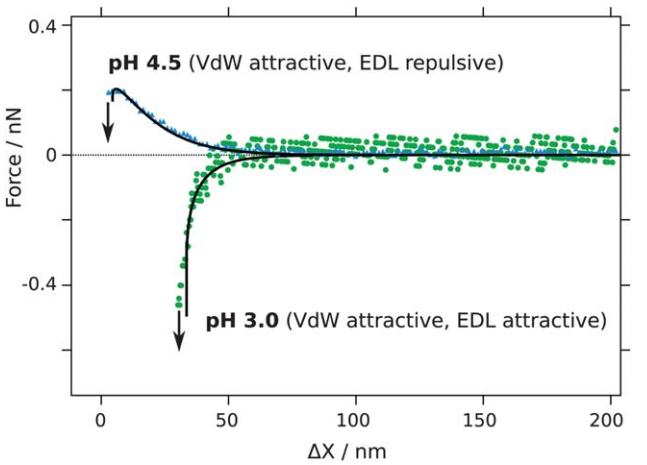

Fig. 5 Effectively equilibrium interactions (at speed = 0.2 μm s^{-1}) between a bubble and PFO droplet measured using the AFM at pH 3.0 and 4.5. Symbols are experimental data points, and solid lines are model predictions generated using the Chan-Dagastine-White model.

For interactions between TD droplets and bubbles, the case becomes more complex. Measured approach interactions are shown in Fig. 6. At the low ionic strengths of pH 3.2 and pH 5, the air-water-TD VdW interaction is still substantially attractive. Hence, for interactions at pH 3.2, both electrical double-layer and Van der Waals forces are attractive (as for air-water-PFO at pH 3.0), and coalescence is observed. At pH 5, the air-water and TD-water interface are both negatively charged (Fig. 4, but the Van der Waals interaction is still overall attractive, which

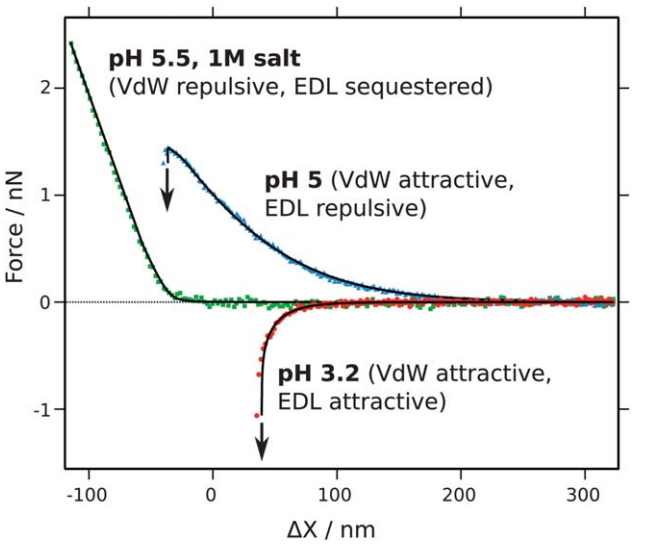

Fig. 6 Effectively equilibrium interactions (at speed = 0.2 μm s^{-1}) between a bubble and TD droplet measured using the AFM in various solution conditions. For interactions at pH 5 and 3.2, the solution ionic strengths were dictated solely by the pH, and hence were 0.05 and 0.63 mM respectively. Symbols are experimental data points, and solid lines are model predictions generated using the Chan-Dagastine-White model.

combine to give a small repulsion followed by coalescence at close approach. For pH 5.5 but with 1 M electrolyte ($NaNO_3$) added, the Hamaker function has been rendered substantially negative which gives a repulsive VdW interaction. At this ionic strength, the Debye length is sufficiently short to render any remaining electrical double-layer interaction shorter in range than the Van der Waals interaction. In this case, the repulsion provided by the Van der Waals interaction is great enough to inhibit coalescence, resulting in a stable collision. The observations presented here are specific to the droplet/bubble sizes used. By using significantly larger bodies, different film thicknesses would be accessed due to the lower Laplace pressures encountered, and hence the behaviour could be different.

Dynamic interactions

A robust and complete framework with which to understand dynamic interactions between deformable bodies in terms of the surface forces, lubrication and deformations has been developed and tested on a number of experimental systems.[5,8,17,20,34] However, thus far, this modelling has only been applied to probe interactions between like pairs of bubbles or drops. The main difference that complicates analysis of the hetero-case presented here is that the two relevant interfaces (oil-water and air-water) have different interfacial tensions. This means that under an applied force as they approach one another, they will tend to deform to different extents. However, by accounting for this additional factor, it is found that a continuum lubrication theory can accurately describe the behaviour of the aqueous film between the interfaces.

Force data as a function of time for dynamic collision interactions between an air bubble on the AFM cantilever and a surface-immobilised PFO droplet are shown in Fig. 7. When the droplet and bubble are far apart (the left hand side of the graph) the bubble and drop do not interact significantly, and no force is experienced. As they approach one another, a film starts to form between the air-water and oil-water interfaces. The hydrodynamic resistance due to water draining from this film manifests as a repulsive force. As the film continues to drain and the droplet and bubble approach more closely, their interfaces deform in response to the repulsive disjoining pressure in the film from hydrodynamic resistance and the overlap of electrical double-layers. In the relatively constant-slope region approaching point **b**, the drop and bubble are deforming (to different extents) and hence the slope of this region is strongly correlated to their interfacial tensions and radii. At a fixed force (point **b**), the piezo begins to retract, and hence the bubble begins to retract from the PFO droplet. As the droplet and bubble are pulled apart, there is a hydrodynamic resistance from water draining back into the film, that causes a 'suction' effect. This manifests as a negative force, acting to pull the interfaces closer together and thin the film. In fact, the draining film attains minimum thickness during the retraction phase. However, the film does not thin sufficiently in these cases to allow coalescence (as the strong repulsion from overlapping electrical double-layers prevents this), so the droplet and bubble are pulled apart and separate from one another.

In order to further understand the behaviour of the two different interfaces during the dynamic interaction, individual

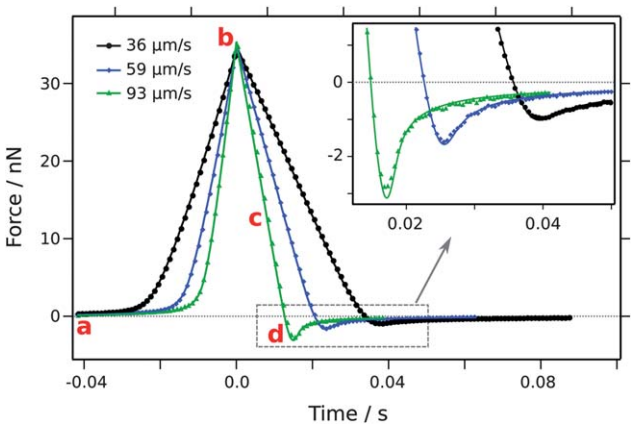

Fig. 7 Dynamic interactions between a bubble and PFO droplet at pH 6.5, measured using the AFM at nominal speeds of 36, 59 and 93 μm s^{-1}. The force is shown as a function of time, and the inset shows the hydrodynamic 'suction' region bounded by the dashed grey box on an enhanced scale. Symbols are experimental data points from the AFM measurement, and solid lines are model predictions generated as described in the text. Time values are offset to be relative to that at the force maximum for clarity of presentation. Lower-case letters refer to specific points of interest in the curve which are shown as deformations in Fig. 8.

deformations of the droplet and bubble were obtained from modeling the interfaces during the collision. It is seen that, as expected, the droplet deforms considerably more at all points than the bubble. This is because the tension of the PFO-water interface (50.5 mN m^{-1}) is lower than that of the air-water interface (72.4 mN m^{-1}), and hence is more deformable when subjected to an applied force. Explicit values of deformations for an approach-retract interaction are shown in Fig. 8. This plot shows deformation of each interface from its equilibrium (spherical cap) geometry as a function of radial dimension. Points in the approach-retract cycle were chosen to best demonstrate the effects of hydrodynamic forces on the interfacial

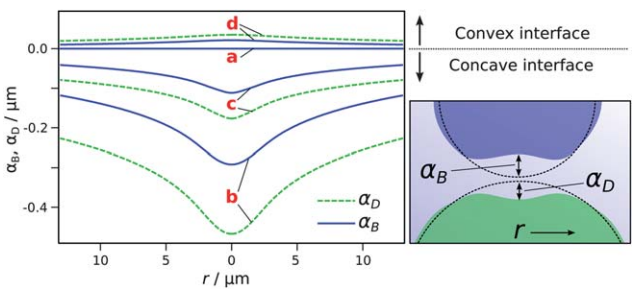

Fig. 8 Left pane: Interfacial deformations of an air bubble and TD droplet, α_B and α_D respectively, during an approach interaction, where the lower-case letters correspond to points in the force *vs.* time data presented in Fig. 7. For each pair of interfaces, the dashed line represents the deformation of the droplet, and the solid line of the air bubble. The deformation is defined as the spatial difference between the deformed interface, and the interface of the spherical, undeformed body, shown schematically in the right pane. Right pane: Shaded shapes show the deformed bodies (deformations not to scale), and the dashed lines represent the equivalent undeformed interfaces, which would be observed if there were no interaction.

profiles of the bubble and droplet. When the droplet and bubble are far apart (shown as point **a** in Fig. 7, and profiles **a** in Fig. 8), no interaction is experienced, and the interfaces remain undeformed. At the point of maximum applied force (**b**), the interfaces are substantially deformed due to the hydrodynamic pressure of water in the film between the two bodies, which is gradually draining. As the bubble is retracted, the film continues to drain, and the interfaces continue to approach one another (**c**). As the interfaces are pulled apart, a suction force is felt (**d**) due to the resistance of water flowing back into the film region, which causes the two interfaces to be pulled toward one another, resulting in an extensional deformation of the droplet and bubble.

Conclusions

Interactions between hetero bubble-drop pairs in aqueous solutions were analysed by first looking at the properties of homo drop-drop and bubble-bubble pairs. It was found that by selection of oil type and solution pH, both electrical double-layer and Van der Waals interactions can be rendered attractive or repulsive. By using this information, bubble-drop pairs can be selectively made stable, or caused to coalesce. Analysis of dynamic interactions between bubble-drop pairs showed that conventional lubrication theory was able to describe the flow of liquid in the thin-film region generated during close approach. All of the experimental results on dynamic forces are consistent with the tangentially immobile boundary condition at the droplet-water and bubble-water interfaces. Use of the conventional zero tangential stress at these interfaces would predict forces that are far to small. Such insight may prove useful in designing the next generation of microfluidic devices which are beginning to incorporate such mixed droplet/bubble systems.

Acknowledgements

X. S. Tang and S. O'Shea are thanked for preparing the cantilevers used. The ARC is thanked for financial support, and the Particulate Fluids Processing Centre, a special research centre of the ARC, provided infrastructure support for the project.

References

1 G. A. van Aken, *Colloids Surf., A*, 2001, **190**, 333–354.
2 M. Niewiadomski, A. V. Nguyen, J. Hupka, J. Nalaskowski and J. D. Miller, *Int. J. Environ. Pollut.*, 2007, **30**, 313–331.
3 S. A. Khan and S. Duraiswamy, *Lab Chip*, 2009, **9**, 1840–1842.
4 S. Duraiswamy and S. A. Khan, *Nano Lett.*, 2010, **10**, 3757–3763.
5 R. R. Dagastine, R. Manica, S. L. Carnie, D. Y. C. Chan, G. W. Stevens and F. Grieser, *Science*, 2006, **313**, 210–213.
6 K. Malysa, *Adv. Colloid Interface Sci.*, 1992, **40**, 37–83.
7 R. F. Tabor, D. Y. C. Chan, F. Grieser and R. R. Dagastine, *Angew. Chem., Int. Ed.*, 2011, **50**, 3454–3456.
8 D. Y. C. Chan, R. Manica and E. Klaseboer, *Soft Matter*, 2011, **7**, 2235–2264.
9 R. F. Tabor, H. Lockie, D. Mair, R. Manica, D. Y. C. Chan, F. Grieser and R. R. Dagastine, *J. Phys. Chem. Lett.*, 2011, **2**, 961–965.
10 D. Y. C. Chan, E. Klaseboer and R. Manica, *Adv. Colloid Interface Sci.*, 2011, **165**, 70–90.
11 C. J. van Oss, *J. Mol. Recognit.*, 2003, **16**, 177–190.
12 Y. S. Djikaev and E. Ruckenstein, *J. Chem. Phys.*, 2009, **130**, 124713–10.
13 T. D. Blake and J. A. Kitchener, *J. Chem. Soc., Faraday Trans. 1*, 1972, **68**, 1435–1442.
14 V. S. J. Craig, B. W. Ninham and R. M. Pashley, *Langmuir*, 1999, **15**, 1562–1569.
15 R. Aveyard and J. H. Clint, *J. Chem. Soc., Faraday Trans.*, 1997, **93**, 1397–1403.
16 S. Biggs and F. Grieser, *J. Colloid Interface Sci.*, 1994, **165**, 425–430.
17 O. Manor, I. U. Vakarelski, G. W. Stevens, F. Grieser, R. R. Dagastine and D. Y. C. Chan, *Langmuir*, 2008, **24**, 11533–11543.
18 I. U. Vakarelski, R. Manica, X. Tang, S. J. O'Shea, G. W. Stevens, F. Grieser, R. R. Dagastine and D. Y. C. Chan, *Proc. Natl. Acad. Sci. U. S. A.*, 2010, **107**, 11177–11182.
19 J. L. Hutter and J. Bechhoefer, *Rev. Sci. Instrum.*, 1993, **64**, 1868–1873.
20 R. Manica, J. N. Connor, R. R. Dagastine, S. L. Carnie, R. G. Horn and D. Y. C. Chan, *Phys. Fluids*, 2008, **20**, 032101–12.
21 I. E. Dzaloshinskii, E. M. Lifshitz and L. P. Pitaerskii, *Adv. Phys.*, 1961, **10**, 165–209.
22 R. R. Dagastine, D. C. Prieve and L. R. White, *J. Colloid Interface Sci.*, 2000, **231**, 351–358.
23 D. B. Hough and L. R. White, *Adv. Colloid Interface Sci.*, 1980, **14**, 3–41.
24 C. J. Drummond, G. Georgaklis and D. Y. C. Chan, *Langmuir*, 1996, **12**, 2617–2621.
25 A. J. Castellanos, M. Garcia-Sucre and G. Urbina-Villalba, *J. Phys. Chem. B*, 2003, **107**, 8532–8537.
26 D. C. Prieve and W. B. Russel, *J. Colloid Interface Sci.*, 1988, **125**, 1–13.
27 V. A. Parsegian and G. H. Weiss, *J. Colloid Interface Sci.*, 1981, **81**, 285–289.
28 R. F. Tabor, R. Manica, D. Y. C. Chan, F. Grieser and R. R. Dagastine, *Phys. Rev. Lett.*, 2011, **106**, 064501/1–4.
29 D. Y. C. Chan, R. R. Dagastine and L. R. White, *J. Colloid Interface Sci.*, 2001, **236**, 141–154.
30 R. R. Dagastine and L. R. White, *J. Colloid Interface Sci.*, 2002, **247**, 310–320.
31 M. Takahashi, *J. Phys. Chem. B*, 2005, **109**, 21858–21864.
32 P. Creux, J. Lachaise, A. Graciaa, J. K. Beattie and A. Djerdjev, *J. Phys. Chem. B*, 2009, **113**, 14146–14150.
33 L. Y. Clasohm, I. U. Vakarelski, R. R. Dagastine, D. Y. C. Chan, G. W. Stevens and F. Grieser, *Langmuir*, 2007, **23**, 9335–9340.
34 H. E. Lockie, R. Manica, G. W. Stevens, F. Grieser, D. Y. C. Chan and R. R. Dagastine, *Langmuir*, 2011, **27**, 2676–2685.
35 J. K. Beattie and A. M. Djerdjev, *Angew. Chem., Int. Ed.*, 2004, **43**, 3368–3571.